

The impact of galaxy formation on X-ray groups

Scott T. Kay,^{1*} Peter A. Thomas¹ and Tom Theuns^{2,3,4}

¹*Astronomy Centre, University of Sussex, Falmer, Brighton BN1 9QJ*

²*Institute for Computational Cosmology, Physics Department, University of Durham, South Road, Durham DH1 3LE*

³*Institute of Astronomy, Madingley Road, Cambridge CB3 0HA*

⁴*Universitaire Instelling Antwerpen, Universiteitsplein 1, B-2610 Antwerpen, Belgium*

Accepted 2003 April 8. Received 2003 March 18; in original form 2002 October 25

ABSTRACT

Using hydrodynamical simulations of the Λ -cold dark matter cosmology that include both radiative cooling and a phenomenological model for star formation and supernovae feedback, we investigate the impact of galaxy formation on the X-ray properties of groups at zero redshift. Motivated by the observed ‘break’ in the L_x – T_x relation at $kT_x \sim 1$ – 2 keV, our feedback model is based on the assumption that supernovae imprint a temperature scale on the hot gas, with the star formation rate and corresponding reheated gas mass then depending only on the available energy budget. We demonstrate that a strong feedback model with a heating temperature comparable to this break ($kT_{\text{SN}} = 2$ keV), and an energy budget twice that available from supernovae ($\epsilon = 2$), raises the core entropy of groups sufficiently to produce an adequate match to their observed X-ray properties. A lower value of ϵ increases the star formation rate without significantly affecting the X-ray properties of groups, and a model with $\epsilon \sim 0.1$ reproduces the observed fraction of baryons in stars. However, a heating temperature that is lower than the virial temperatures of the groups leads to an excess of cooling gas that boosts their X-ray luminosities, due to the failure of the reheated material to escape from the gravitational potential. A limited study of numerical resolution effects reveals that the temperature of poorly resolved objects is underestimated, therefore (in our case) a fully resolved group population would lead to a steeper L_x – T_x relation, bringing our results into even better agreement with the observations.

Key words: hydrodynamics – methods: numerical – galaxies: formation – X-rays: galaxies: clusters.

1 INTRODUCTION

Groups¹ are the most common agglomerates of galaxies in the low-redshift universe and also harbour the majority of currently detected baryons (Fukugita, Hogan & Peebles 1998), observed because of their emission of soft X-rays ($kT \sim 0.1$ – 1 keV). The simplest explanation for the properties of this gas is that it was shock-heated during the gravitational collapse and virialization of the system. For self-similar ($\Omega = 1$) systems, this leads to a simple scaling between X-ray luminosity and temperature, $L_x \propto T^{3/2}(1+z)^{3/2}\Lambda(T)$, where $\Lambda(T)$ denotes the cooling rate of the gas.

In the largest clusters, the virial temperature is sufficiently high that the gas predominantly emits bremsstrahlung radiation, leading to the scaling $L_x \propto T^2$ (Kaiser 1986). This result was recently vindicated by Allen, Schmidt & Fabian (2002) using high-quality

Chandra data. In smaller systems, the increasing importance of line emission boosts the luminosity and so should flatten the L_x – T_x relation. Observationally the converse is true, with the slope of the relation for low-mass groups being as high as ~ 6 (e.g. see Xue & Wu 2000 for a recent compilation). This result is also reflected in the low amplitude of the soft X-ray background – around an order of magnitude lower than predicted from gravitational heating models (e.g. Pen 1999; Bryan & Voit 2001; Wu, Fabian & Nulsen 2001).

Evrard & Henry (1991, see also Kaiser 1991; Bower 1997; Voit et al. 2002) argued that the deficit in luminosity is due to additional physical processes raising the *entropy* of the gas. (Entropy is invariant under adiabatic processes, making it a useful variable for characterizing the effects of cooling and heating on the gas distribution.) Gravitational heating leads to the mean entropy of a self-similar system scaling as $s \propto T/(1+z)^2$.² Increasing the entropy of the gas corresponds to a hotter but less-concentrated distribution.

*E-mail: s.t.kay@sussex.ac.uk

¹We use the term ‘groups’ to mean systems with X-ray temperatures of the order of 1 keV or lower.

²We use the term *entropy* to mean $s = T/\rho^{\gamma-1}$, and assume $\gamma = \frac{5}{3}$, for a monatomic ideal gas.

Consequently, for a given increase in entropy, the X-ray emissivity is lowered preferentially in low-mass systems, steepening the L_x-T_x relation. Ponman, Cannon & Navarro (1999) measured the entropy of groups and clusters at 10 per cent of their virial radii, and showed that low-mass clusters and groups deviated from the self-similar prediction, tending to a constant value of $\sim 100 h^{-1/3}$ keV cm² (albeit with very large scatter).

The precise origin of the excess entropy is still unclear, but is most probably a direct consequence of the galaxy formation process (Evrard & Henry 1991). For example, galactic winds from supernovae (SNe) explosions and/or active galactic nuclei (AGN) could heat the gas, raise its entropy and allow it to convect out to lower-density environments. Winds have already been observed in low-redshift starburst (e.g. Heckman 2000) and high-redshift Lyman break galaxies (e.g. Pettini et al. 2001), and the presence of metal-enriched gas in low-density regions suggests galactic material has been expelled from haloes (e.g. Schaye et al. 2000). Note that in hierarchical models, at least some heating (feedback) is required in order to regulate the star formation rate (e.g. White & Rees 1978; Balogh et al. 2001).

The amount of *energy* required to generate excess entropy depends on the environment. If the gas was close to mean density when heated (the *pre-heating* scenario) only ~ 0.3 keV of energy per particle is required (Lloyd-Davies, Ponman & Cannon 2000). More realistically, if the heating occurred in high-density regions, as much as 1–3 keV per particle is required (e.g. Kravtsov & Yepes 2000; Wu, Fabian & Nulsen 2000; Borgani et al. 2002; Bower et al. 2001). Note, however, that the total energy production is smaller in the latter case as only gas in the cores of haloes need be heated.

Excess entropy is also generated by the process of star/black hole formation itself, removing cold, low-entropy material and causing higher-entropy material to flow in to replace it (Knight & Ponman 1997). Models using only radiative cooling to generate the excess entropy have been implemented by a number of authors, and have proved successful in reproducing a number of X-ray scaling relations (e.g. Bryan 2000; Pearce et al. 2000; Muanwong et al. 2001; Voit & Bryan 2001; Davé, Katz & Weinberg 2002; Muanwong et al. 2002; Wu & Xue 2002a,b). Voit & Bryan (2001) demonstrated that the entropy–temperature locus of gas with a range of temperatures and densities set by equating their cooling times to the age of the Universe, closely matches the relation observed by Ponman et al. (1999). Voit & Bryan further argued for the presence of an entropy *floor* by asserting that cooled gas will either form stars or be heated (by stars or AGN) and move to a higher adiabat.

The aim of this paper is to investigate how galaxies that form in a cosmological simulation impact upon the X-ray properties of groups. This treatment allows us to incorporate cooling and heating processes in a self-consistent manner. Specifically, we include the effects of both radiative cooling/star formation and feedback of energy from supernovae in our simulations, but neglect an AGN component (although in broad terms, the effects of including AGN may largely mimic the desired effects of supernovae, since both are ultimately powered by cooling gas). Motivated by the observed ‘break’ in the L_x-T_x relation at the interface between groups and clusters ($kT \sim 1-2$ keV), our feedback model is fundamentally based on the assumption that cold gas is reheated to a fixed temperature and the mass ratio of reheated gas to stars is determined by the overall energy budget. As we shall see, our model is able to reproduce the required entropy excess, provided that the heating temperature is sufficiently high to allow the majority of reheated gas to escape from haloes, while varying the energy budget primarily controls the fraction of baryons in stars.

We organize the remainder of this paper as follows. In Section 2 we outline our method, giving details of the simulations as well as our approach to cooling, star formation and feedback. Section 3 presents the predicted X-ray group scaling relations for our fiducial simulation at $z = 0$. In Section 4 we investigate our feedback model in more detail, concentrating on the effects of varying parameters. In Section 5, we perform a limited study of numerical resolution effects and summarize our conclusions in Section 6.

2 SIMULATION DETAILS

2.1 Overview

Results are presented for the currently favoured Λ -cold dark matter (Λ CDM) cosmology, setting the density parameter, $\Omega_m = 0.35$, Hubble constant, $h = H_0/100 \text{ km s}^{-1} \text{ Mpc}^{-1} = 0.71$, cosmological constant, $\Omega_\Lambda = \Lambda/3H_0^2 = 0.65$, baryon density, $\Omega_b = 0.038$, and power spectrum normalization, $\sigma_8 = 0.7$. The latter value, recently measured from both cluster abundances (e.g. Seljak 2002) and galaxy clustering (Lahav et al. 2002), is around 20 per cent lower than previous determinations that deduced $\sigma_8 \sim 0.9$ (although, weak lensing statistics still prefer the higher value; see, e.g., Refregier, Rhodes & Groth 2002). We find that increasing σ_8 from 0.7 to 0.9 has only a small effect on the results presented in this paper, but the lower value gives us a numerical advantage, requiring fewer time-steps to evolve to $z = 0$.

Simulation data were generated using a parallel (OpenMP) version of the HYDRA code (Couchman, Thomas & Pearce 1995; Theuns et al. 1998), a combination of the AP³M algorithm (Couchman 1991) to compute gravitational forces and smoothed particle hydrodynamics (SPH; see Monaghan 1992) to calculate gas forces. For the gas, neighbour lists were computed using the recursive binning technique described in Theuns et al. (1998), allowing the density to be estimated for gas particles in low-density regions. SPH forces were calculated using an artificial viscosity based on pairwise particle separations (Monaghan 1992) rather than the local velocity divergence. Our SPH implementation now also includes the force-correction terms suggested by Springel & Hernquist (2002), resulting in improved entropy conservation.

Initial conditions were generated using the COSMIC package supplied with the publicly available version of HYDRA. We made a small modification to COSMIC so that the large-scale structure is preserved when increasing the numerical resolution. For our main results, we adopted a comoving box size of $50 h^{-1}$ Mpc, populated with a perturbed grid of 2097 152 (128^3) dark matter and gas particles each. (Note that the box size is large enough to give statistically meaningful results; Bryan & Voit 2001.) These choices set our gas and dark matter particle masses to $m_{\text{gas}} = 6.3 \times 10^8 h^{-1} M_\odot$ and $m_{\text{dark}} = 5.2 \times 10^9 h^{-1} M_\odot$, respectively. We have chosen this resolution so as not to expect significant heating of the gas due to two-body encounters with the dark matter particles (Steinmetz & White 1997). Gravitational forces were softened on short scales using a spline kernel with an equivalent Plummer softening length of $\epsilon_p \equiv \epsilon_s/2.34 = 10 h^{-1}$ kpc. Gas forces were also limited by fixing the minimum SPH smoothing radius to the gravitational softening $2h_{\text{min}} = \epsilon_s$.

All but the smallest runs were performed on the UK Cosmology Consortium COSMOS Origin 3800 supercomputer in Cambridge, using between 10 and 20 processors. Simulations were started at $z = 49$ and evolved to $z = 0$, typically taking between 2000 and 4500 steps, depending on the choice of resolution and feedback model.

2.2 Radiative cooling and star formation

Radiative cooling was implemented following the method of Thomas & Couchman (1992), using tabulated cooling rates given by Sutherland & Dopita (1993). For the present paper, we adopt a global metallicity scaling law, $Z = 0.3(t/t_0) Z_\odot$, to approximate the gradual enrichment of the intergalactic medium. In principle, we could model metal enrichment self-consistently, since it is a by-product of the supernovae explosions. (We have already performed this to study the impact of dwarf galaxies on the high-redshift intergalactic medium; Theuns et al. 2002.) In order to simplify matters, however, we have decided to leave such a study to a subsequent paper.

We follow the star formation prescription used by Kay et al. (2002, hereafter K2002), converting gas with $\delta > 5000$ and $T < 50\,000$ K into stars at the end of each time-step. This density threshold is low compared with measured empirical density thresholds in galaxies (e.g. Kennicutt 1998), but is close to our resolved density maximum. Increasing the density threshold above the resolution threshold induces a delay to the star formation, increasing the gas-to-stars ratio within each galaxy (K2002).

Subsequent to the star formation routine, we identify groups of 10 stars within the current gravitational softening length and merge them into a single *galaxy fragment*. These fragments are comparable in mass to the dark matter particles and the reduction in the number of particles provides a modest decrease in the CPU time per step.

2.3 Feedback

The essence of any feedback model is to create a diffuse hot phase which powers a wind, providing a mechanism to transport gas away from star-forming regions. However, explicitly modelling a multi-phase medium in a cosmological simulation is impossible because of its limited resolution. This problem has prompted two approaches to implementing feedback within such simulations.

One method is to assume that each resolution element (in the case of SPH, a single gas particle) is representative of a multiphase medium (cold and hot gas and stars), and to solve explicitly for the flux of material between each phase, using a set of physical arguments as laid out by McKee & Ostriker (1977). This approach has been implemented and proved effective by various authors, using both grid-based codes (e.g. Yebes et al. 1997) and SPH (e.g. Hultman & Pharasyn 1999; Springel & Hernquist 2003). The main advantage of this method is that it does not depend explicitly on numerical resolution, and so should be less sensitive to discreteness effects. On the other hand, the phases cannot move independently (although see Springel & Hernquist 2003).

An alternative approach, which we take here, is to allow each particle to represent only one phase and use a set of simple rules to overcome any associated discreteness problems. This has the advantage of being much simpler to implement than the previous method and allows each phase to move freely. K2002 reviewed a number of feedback models within this context; in this paper, we consider an improved version of the thermal feedback approach studied by K2002 and outline details of this method below.

2.3.1 Feedback energetics

The amount of energy available from each star particle at time, t , to heat the gas over a time-step, Δt , is

$$E_{\text{SN}} = 10^{51} \epsilon \left(\frac{m_*}{M_\odot} \right) \int_{t-t_0}^{t+\Delta t-t_0} [r_{\text{Ia}}(\tau)/2 + r_{\text{II}}(\tau)] d\tau \epsilon, \quad (1)$$

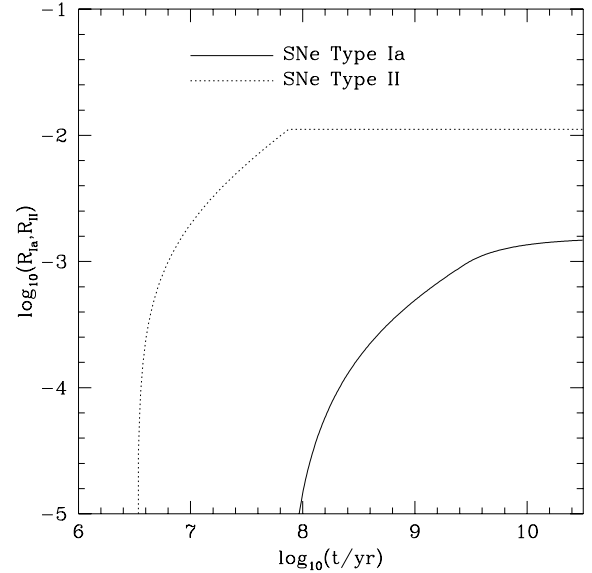


Figure 1. Cumulative number of supernovae per solar mass of stars formed versus time since the star formation episode, using power-law fits of Lia et al. (2002) and assuming a Salpeter IMF.

where m_* is the mass of a star particle, t_0 is the star formation time and r_{Ia} and r_{II} are the rates of Type Ia and Type II supernovae per solar mass of stars formed. (We assume each Type Ia supernova contributes half the energy of a Type II supernova.)

Lia, Portinari & Carraro (2002) tabulated $r(\tau)$ for various initial mass functions (IMF), using the Padova stellar evolutionary tracks (Portinari, Chiosi & Bressan 1998). We adopt the Lia et al. rates for a Salpeter IMF (given in their table 2) and illustrate integrated versions in Fig. 1. The contribution from Type II SNe rises dramatically after approximately 3 Myr, lasting for around 70 Myr. Type Ia SNe start contributing later, at around 100 Myr, but are still declining after 10 Gyr. The total number of Type II SNe is around an order of magnitude higher than the number of Type Ia SNe, and so provides the dominant source of feedback of energy to the interstellar medium.

The parameter ϵ modulates the overall energy available from the SNe, which we term the feedback efficiency. Thornton et al. (1998) suggested that the maximal value ($\epsilon = 1$) may be at least a factor of 5 too high once radiative losses are accounted for. As we shall see in Section 4, our model does not necessarily require a high value of ϵ to generate the required excess entropy; varying this parameter primarily alters the fraction of baryons in galaxies.

2.3.2 Feedback implementation

The thermal feedback model studied by K2002 is effective in reducing the masses/luminosities of galaxies but fails to reproduce the X-ray scaling relations of groups. In their model, each star particle distributes the energy available at each time-step (equation 1) over the surrounding gas. For equal mass particles, the maximum amount of energy a gas particle can receive from a single star particle is enough to heat it by ~ 2 keV (for $\epsilon = 1$). In practice, gas particles escape before receiving this amount of energy and the result is an average heating temperature around an order of magnitude lower. Much of this gas then fails to escape from group and cluster-sized haloes with comparable or higher virial temperatures, and instead

recools, boosting their X-ray luminosities (we will demonstrate this effect in Section 4).

We have devised an alternative method with the clear intention of heating the gas to a higher temperature without necessarily increasing the available energy. In the context of X-ray scaling relations, our new model is motivated by the presence of a ‘break’ in the L_x-T_x relation at $kT_x \sim 1-2$ keV; such a feature may be an imprint of a temperature scale introduced by the heating mechanism. We base the model on the physical assumption that as more and more supernovae go off, it is not the temperature of the gas that is progressively increased (as in the previous method), but the mass fraction of material converted from the cold phase to the hot phase. To implement such a model, we equate the available energy from a mass of newly formed stars, m_* , to the energy required to raise the temperature of a mass of cold gas, δm_{gas} by a fixed amount, T_{SN}

$$\delta m_{\text{gas}}(3kT_{\text{SN}}/2\mu m_{\text{H}}) = E_{\text{SN}}, \quad (2)$$

where E_{SN} is given in equation (1) and we set $\mu m_{\text{H}} = 10^{-24}$ g, the mean molecular weight of a gas with $Y = 0.24$, $Z = 0$. In practice, T_{SN} is much greater than the temperature of the cold gas ($\sim 10^4$ K), so the heating introduces a temperature scale to the hot gas.

Assuming now that m_* is the mass of a star particle, the fractional mass of a gas particle capable of being heated to T_{SN} is

$$f_{\text{heat}} = \frac{\delta m_{\text{gas}}}{m_{\text{gas}}} = 0.209\epsilon \left[\frac{R(t - t_0, \Delta t)}{0.001} \right] \left(\frac{kT_{\text{SN}}}{\text{keV}} \right)^{-1}, \quad (3)$$

using the fact that $m_* = m_{\text{gas}}$ in our method and $R(t - t_0, \Delta t)$ is the integral on the right-hand side of equation (1). (For a typical time-step, $\Delta t \sim 5 \times 10^6$ yr, $\langle R \rangle \sim 0.001$.) Note that in K2002’s model, $f_{\text{heat}} = 1$ and kT_{SN} is calculated, the opposite of our model. For every star particle, we calculate the radius that encloses 32 gas particles, and (since generally $f_{\text{heat}} < 1^3$) apply equation (3) to the first gas particle within this radius with $T < 50\,000$ K. Since each gas particle represents only one phase in our simulations, we can only heat the whole particle to a temperature T_{SN} or not heat it at all. To mimic the effect of heating a fraction of the gas, we draw a random number for each particle, $0 \leq r \leq 1$, and heat it to T_{SN} if $f_{\text{heat}} < r$.

For our fiducial model, for which we present results in the next section, we set $\epsilon = 2$ and $kT_{\text{SN}} = 2$ keV, twice the maximum available energy from standard supernovae calculations, but in reasonable agreement with that suggested in previous studies (e.g. Kravtsov & Yepes 2000; Bower et al. 2001; Wu et al. 2001; Borgani et al. 2002). As we will show, this model predicts X-ray properties of groups in good agreement with the data. We will demonstrate in Section 4, however, that a good match to the scaling relations is reasonably insensitive to this choice of ϵ , but does require the heating temperature to be sufficiently high in order for gas to escape from the gravitational potential of the halo. The fiducial temperature, which is significantly larger than typically found when using K2002’s model, also alleviates the need for preventing gas from cooling radiatively over a fixed period of time (as implemented by K2002), because cooling gas only starts to become thermally unstable at lower temperatures ($kT \sim 0.2-1$ keV for $Z = 0-0.3 Z_{\odot}$).

³Exceptions to this rule can occur if $\epsilon/kT_{\text{SN}} > 5$; this is true for only one model considered in this paper, where $\epsilon = 1$ and $kT_{\text{SN}} = 0.1$ keV. As we shall see, however, this particular model fails because kT_{SN} is too low, not because less gas is reheated.

3 X-RAY PROPERTIES OF GROUPS IN THE FIDUCIAL MODEL

We begin by demonstrating that our fiducial feedback model provides an adequate match to current observational data at $z = 0$, given the level of uncertainty in these measurements.

Our group catalogues are constructed using the procedure outlined by Muanwong et al. (2002, hereafter M2002), where full details may be found. To summarize, spheres of baryon and dark matter particles are located with constant mean internal overdensity, Δ , relative to the comoving critical density. For our chosen cosmology, $\Delta = 111$ is approximately the value predicted by the spherical top-hat collapse model for a virialized sphere (Eke, Navarro & Frenk 1998). Unless specified, we set $\Delta = 200$ for our main results, but note that the X-ray properties are insensitive to using $\Delta = 200$ rather than $\Delta = 111$. Only objects containing at least 500 baryon plus 500 dark matter particles are retained, setting a minimum halo mass of $2.9 \times 10^{12} h^{-1} M_{\odot}$. At $z = 0$, our fiducial catalogue contains 172 objects.

Once the catalogues were generated, it was found that a small fraction (~ 5 per cent) of groups have X-ray temperatures very much in excess of the average for their mass (i.e. there are hot outliers on the temperature–mass relation). On inspection, these objects are infalling subclumps on the outskirts of larger groups, but have hot gas that has been shocked to the temperature of the more massive object. We choose to eliminate these objects by setting the requirement that each group in the catalogue has an X-ray temperature less than twice the mean value for its mass.

3.1 Entropy

The effect of the removal of hot gas from a halo on its X-ray properties can best be characterized by the change in entropy of the gas. As the hot gas is depleted, higher entropy material flows inwards and is adiabatically heated (i.e. it develops a hotter, less concentrated distribution) in order to maintain gravitational support. This leads to a rise in the X-ray temperature of the gas but a *decrease* in its X-ray luminosity (Knight & Ponman 1997; Pearce et al. 2000). Ponman et al. (1999) demonstrated that lower temperature objects have shallower surface brightness profiles and consequently larger excess entropies, relative to the expected self-similar relation for a model neglecting galaxy formation (we refer to this as a *non-radiative* model).

Following Ponman et al. we measure the entropy of each object at $0.1r_{\text{vir}}$ as a function of X-ray temperature. The latter is evaluated within a soft band of energy range 0.3–1.5 keV,

$$T_x = \frac{\sum_i m_i \rho_i \Lambda_{\text{soft}}(T_i, Z) T_i}{\sum_i m_i \rho_i \Lambda_{\text{soft}}(T_i, Z)}, \quad (4)$$

where the sum is performed over all hot gas particles ($T > 10^5$ K) within the virial radius of the group, each with mass m_i , density ρ_i and temperature T_i . The soft-band cooling function, Λ_{soft} is calculated using the models of Raymond & Smith (1977). We then estimate the entropy of each group

$$s_x = kT_x / \langle n_e \rangle^{2/3}, \quad (5)$$

where

$$\langle n_e \rangle = \frac{\eta}{m_{\text{H}}} \frac{3M}{4\pi r^2 \delta r} \quad (6)$$

is the electron density, averaged over all hot gas particles (of total mass, M) within a shell of width, $\delta r = 0.1r_{\text{vir}}$, centred on

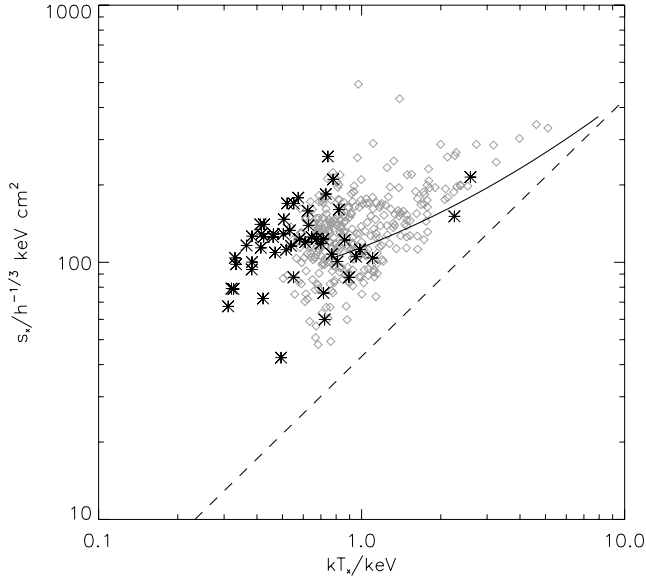


Figure 2. Core entropy (measured at $0.1r_{\text{vir}}$) against X-ray temperature. Stars represent groups in the fiducial model and diamonds from the *radiative* simulation in M2002. The solid line represents the trend observed by Ponman et al. (1999) and the dashed line is a fit to the self-similar relation obtained from *non-radiative* simulations.

$r = 0.1r_{\text{vir}}$. Only groups containing 10 or more particles within this region are plotted. We set the number of electrons per baryon, $\eta = 0.88$, appropriate for a primordial gas ($Y = 0.24$, $Z = 0$), although insensitive to the assumed range of Z .

Fig. 2 shows the simulated entropy–temperature relation (stars), as well as groups/clusters from the *radiative* simulation studied by M2002 (diamonds). Our fiducial model agrees well with M2002’s result where the two samples overlap, as well as with the general trend observed by Ponman et al. (solid curve), clearly demonstrating an entropy in excess of the self-similar prediction ($s_x \propto T_x$, dashed line). The increasing impact of the galaxies with decreasing halo mass leads to an increase in the excess entropy, consistent with the expectation of an entropy floor at $s_x \sim 100 h^{-1/3} \text{ keV cm}^2$.

3.2 X-ray temperature

Increasing the entropy of the gas leads to a higher X-ray temperature at fixed mass, resulting in an increase in the normalization of the temperature–mass relation (e.g. Muanwong et al. 2001; Thomas et al. 2002). We plot the fiducial temperature–mass relation in Fig. 3 (stars), with the solid line representing a least-squares fit to the data. The square points show the result of excluding emission from within the cooling radius⁴ of each object. This has the effect of slightly increasing the temperatures of some of the larger objects, without significantly affecting the slope or normalization of the relation.

The result is in reasonable agreement with the *radiative* model studied by M2002 (diamonds), but predicts a flatter relation ($T_x \propto M_{200}^{1/2}$ as opposed to $T_x \propto M_{200}^{0.6}$). Lower-mass groups have X-ray temperatures in excess of their virial temperatures ($T_{\text{vir}} \propto M_{200}^{2/3}$, dotted line), as expected from the increase in entropy of these systems. In the highest-mass group, the presence of cooler reheated gas within the virial radius biases its X-ray temperature lower than the

⁴The cooling radius is defined as that which encloses hot gas with an average cooling time equal to 6 Gyr.

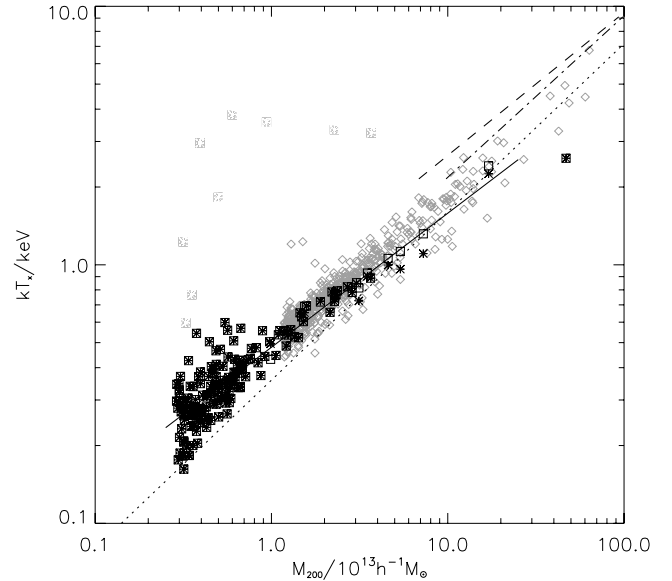


Figure 3. X-ray temperature–mass relation for the fiducial model (stars). Temperatures calculated when excluding particles from within the cooling radius are shown as squares. Also plotted is the M2002 *radiative* sample (diamonds). The dotted line is the relation between virial temperature and mass. Dashed and dot-dashed lines represent best-fitting relations to the observational data presented in Xu et al. (2001) for NFW and β model surface brightness profiles, respectively.

virial temperature. It is possible that a good fit to higher-mass systems will require an even higher heating temperature than employed here.

The dashed and dot-dashed lines in Fig. 3 represent power-law fits to the observed temperature–mass relation for clusters, compiled by Xu, Jin & Wu (2001), using NFW and β model surface brightness profiles, respectively. Both fits are offset from the simulated relation by up to 40 per cent. A likely reason for this offset is that the masses are underestimated when extrapolating X-ray surface brightness profiles to the virial radius. M2002 demonstrated that by estimating cluster masses in this way (assuming a relation between the observable extent of an object and its true size) the resulting temperature–mass relation was in much closer agreement with the observations. This conclusion was strengthened when the same data set was shown to be in good agreement with the temperature–mass relation for a sample of high-resolution clusters observed with the *Chandra* satellite (Allen et al. 2002), for masses measured within a density contrast of 2500 (Thomas et al. 2002).

For groups, the problem of estimating masses from the X-ray data is exacerbated by their lower surface brightness, and so galaxy velocity dispersion is commonly used as an independent measure of the dynamical size of the halo from its temperature. We plot the relation between X-ray temperature and dark matter velocity dispersion, σ_{DM} , for our fiducial model in Fig. 4. (Numerical resolution limits the number of galaxies per halo to a few in most cases, preventing us from reliably estimating the galaxy velocity dispersion. Previous simulations have shown that the galaxies trace the potential reasonably well, see, e.g., Springel et al. 2001; Davé et al. 2002.)

The dot-dashed line shows the expected relation if the gas contained the same specific energy as the dark matter, i.e. $T_x \propto \sigma_{\text{DM}}^2$. Again, the larger X-ray temperatures of the smaller groups flattens this relation, resulting in $T_x \propto \sigma_{\text{DM}}^{3/2}$ (solid line). To quantify this effect, we plot the ratio of specific energies between the hot gas and

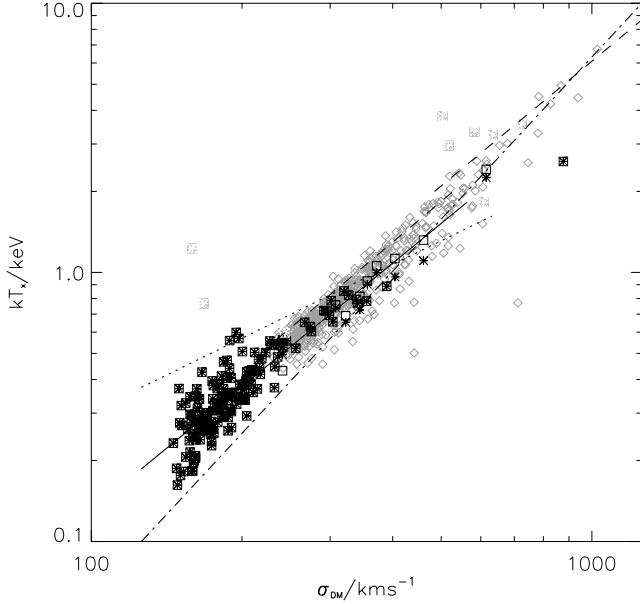


Figure 4. X-ray temperature against dark matter velocity dispersion for groups in the fiducial model (stars). Square points are for when emission is excluded from within the cooling radius (with the solid line representing a least-squares fit to these objects). Diamonds are from the *radiative* simulation studied by M2002. The dot-dashed line is the expected relation when the gas and dark matter have equal specific energies ($T \propto \sigma^2$). Dotted and dashed lines represent best fits to the group data in Helsdon & Ponman (2000) and the compiled group and cluster data in Xue & Wu (2000).

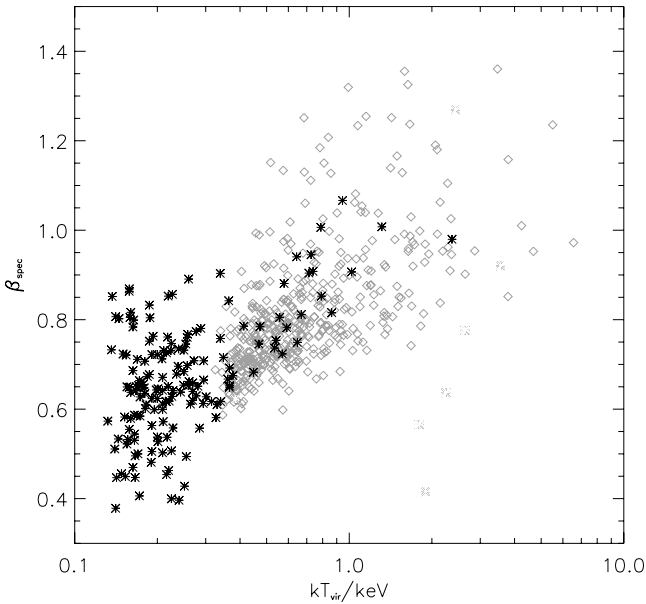


Figure 5. The ratio between X-ray temperature and dark matter velocity dispersion, β_{spec} , versus virial temperature for groups in the fiducial model (stars). Diamonds are from the *radiative* simulation studied by M2002.

the dark matter

$$\beta_{\text{spec}} = \frac{\mu m_{\text{H}} \sigma_{\text{DM}}^2}{k T_{\text{x}}}, \quad (7)$$

in Fig. 5. The smaller objects contain, on average, X-ray luminous gas that is nearly twice as hot as the dark matter. For the higher-

mass objects ($kT_{\text{vir}} > 1$ keV), however, the two components are approximately at the same temperature.

Also plotted in Fig. 4 are the best fits to the group data presented in Helsdon & Ponman (2000, dotted line), and the group and cluster data compiled by Xue & Wu (2000, dashed lines). The Helsdon–Ponman relation is much flatter than the Xue–Wu line, due to their sample containing several low-temperature groups with low-velocity dispersions. Removing these outliers from the sample would result in closer agreement with Xue & Wu’s relation. Our simulated relation reproduces Xue & Wu’s observational determination, $T_{\text{x}} \propto \sigma_{\text{gal}}^{1.56}$, reasonably well.

3.3 X-ray luminosity

The increase in entropy decreases the X-ray luminosity of groups. Since this has a greater effect on less massive objects, it leads to a steepening of the $L_{\text{x}}-T_{\text{x}}$ and $L_{\text{x}}-\sigma$ relations, which we will quantify here.

As in M2002 we estimate bolometric X-ray luminosity by applying a correction to the soft-band emissivity

$$L_{\text{x}} = \frac{\Lambda_{\text{bol}}(T_{\text{x}})}{\Lambda_{\text{soft}}(T_{\text{x}})} \sum_i \frac{m_i \rho_i \Lambda_{\text{soft}}(T_i, Z)}{(\mu m_{\text{H}})^2}, \quad (8)$$

where T_{x} is calculated using equation (4), Λ_{bol} is the bolometric cooling function used in the simulations (see Section 2).

Figs 6 and 7 illustrate the $L_{\text{x}}-T_{\text{x}}$ and $L_{\text{x}}-\sigma$ relations, respectively, for the fiducial simulation. Again, the model agrees reasonably well with both M2002’s result and the observed relations, given the uncertainty in the latter. Furthermore, increasing the resolution of the smaller objects (which are less well resolved than the larger groups) increases their temperature, which will bring the $L_{\text{x}}-T_{\text{x}}$ relation into better agreement with the observed relation (see Section 5). Note that the ‘break’ in the relation at around

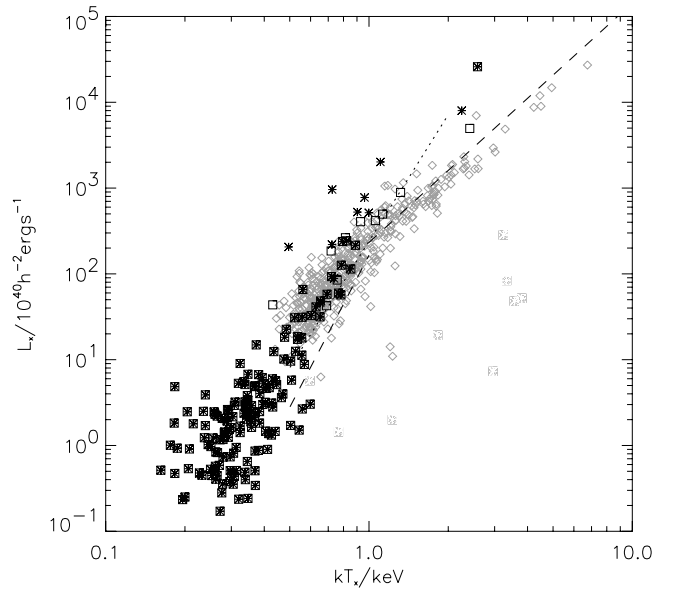


Figure 6. Luminosity–temperature relation for groups in the fiducial model (stars). Square points are the result when emission from within the cooling radius is excluded. Diamonds are from the *radiative* simulation studied by M2002. Dashed lines represent the best-fitting relations to the group and cluster samples compiled by Xue & Wu (2000). The dotted line illustrates the best-fitting power law to the sample of groups found by Helsdon & Ponman (2000).

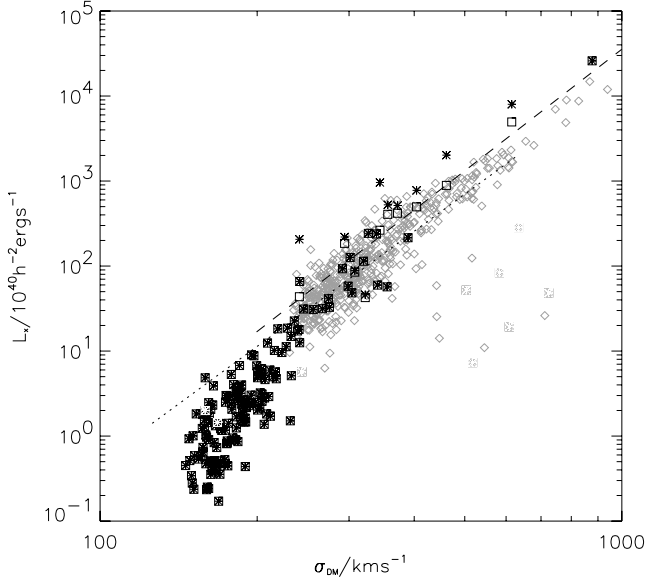


Figure 7. L_x – σ_{DM} relation for groups in the fiducial model (stars). Square points are the result when emission from within the cooling radius is excluded. Diamonds are from the *radiative* simulation studied by M2002. Dashed lines represent the best-fitting relations to the group and cluster samples compiled by Xue & Wu (2000). The dotted line illustrates the best-fitting power law to the sample of groups found by Helsdon & Ponman (2000).

1 keV is more prominent in the L_x – T_x relation than in the L_x – σ relation, due to the additional effect of entropy increase on temperature, causing the relation to steepen further.

3.4 Baryon fractions

Although cooling and heating (feedback) are both mechanisms for increasing the core entropy of groups, they have opposing effects on the stellar baryon fraction. Cooling acts to increase and feedback decrease galaxy masses, hence matching the observed value requires a balance between the two processes. Cooling and feedback can also have different effects on the hot gas fractions. Although cooling reduces the hot gas content, feedback can cause an increase (reheated gas that has not moved beyond the virial radius) or a decrease (transfer of energy between outflows and hot halo gas increases the fraction expelled from the halo).

In Fig. 8 we plot mass fractions of baryons, in units of the global value (Ω_b/Ω_m), against the virial temperature of each halo for the fiducial model (filled symbols) and M2002’s *radiative* simulation (open symbols). The total baryon fractions are plotted in Fig. 8(a). Both models appear to be converging towards a value close to unity at high virial temperatures, but the baryon fractions decrease much more rapidly at lower temperatures when feedback is included. The difference between baryon fractions reflects the total amount of gas expelled from the halo by feedback.

The baryon fractions are split into hot gas ($T > 10^5$ K, diamonds) and cold gas + star (triangles) fractions in Fig. 8(b). The same trend is present between the two models for the cooled baryon fractions (since galaxy formation efficiency is higher in smaller objects, where average cooling times are shorter), but the values at a given temperature are different. The cooled fraction is twice as high in the M2002 objects, and could be higher: the absence of feedback in this simulation means that only the numerical resolution limited these

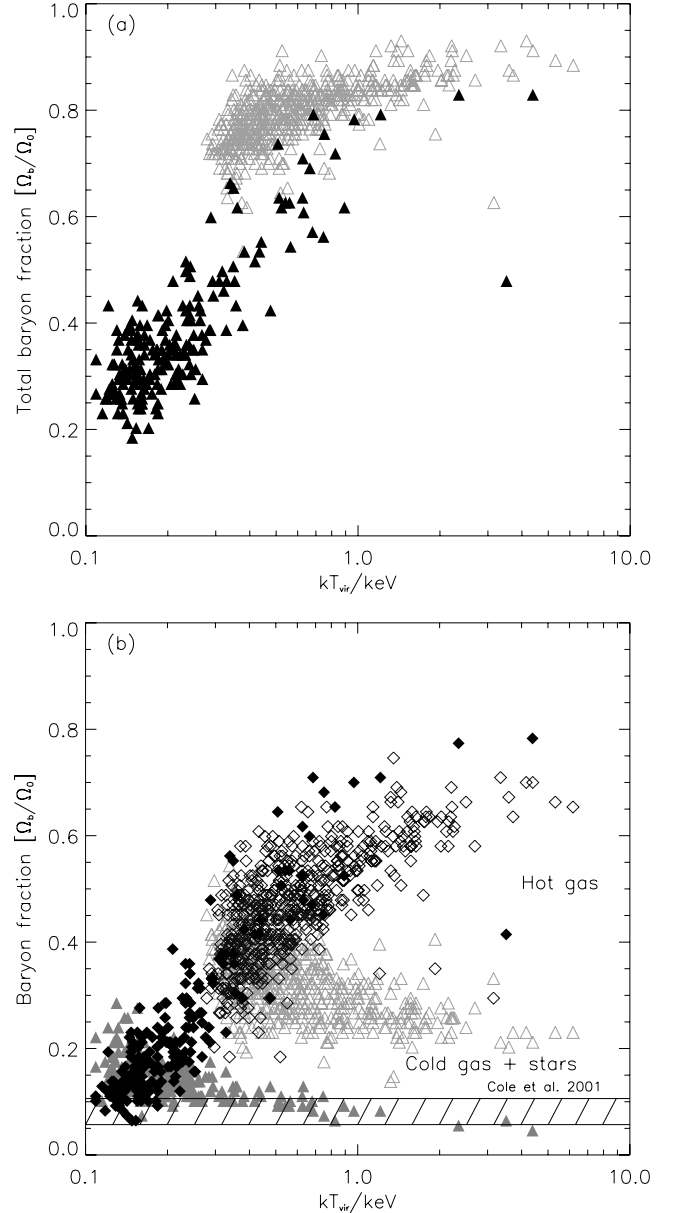


Figure 8. Baryon fractions, in units of the global value, against virial temperature for groups in the fiducial simulation (filled symbols) and in the *radiative* simulation studied by M2002 (open symbols). Total baryon fractions are plotted in (a), separated into hot gas (diamonds) and cold gas + stars (triangles) in (b). The shaded region represents the two global cooled fractions measured by Cole et al. (2001) for the Salpeter (upper horizontal line) and the Kennicutt (lower line) IMF.

values. Feedback also steepens the relation between the hot gas fraction and virial temperature. As we discuss in Section 4, objects with virial temperatures above the feedback temperature, kT_{SN} , retain a fraction of reheated gas that slightly increases their hot gas fraction. In smaller systems, however, feedback has a larger impact on the hot gas, expelling a significant fraction from the halo.

The shaded region in Fig. 8 represents measured global cooled gas fractions (the global value is the asymptotic limit for a large halo mass), combining the stellar fractions measured by Cole et al. using data from the 2MASS and 2dF galaxy surveys, with a further 10 per cent of the mass in cold gas (Balogh et al. 2001). The upper horizontal line represents the value determined when using the Salpeter IMF

(as used in our feedback model) and the lower line for the Kennicutt IMF. Globally, only just over 3 per cent of the gas forms stars in the fiducial model by $z = 0$, lower than the observed value by a factor of ~ 3 . Increasing the resolution does not significantly increase the cooled fraction (Section 5) because feedback acts to stabilize this quantity and our simulation has already resolved the majority of the galaxy mass density. As we discuss in the next section, however, a higher cooled fraction can be achieved by choosing a lower ϵ , which does not significantly affect the scaling relations. Additionally, increasing the metallicity of cooling gas will increase the fraction of baryons in stars. The metallicity of high-density regions has been underestimated in our simulation since stars in galaxies at the present day have been enriched to solar abundance (Edmunds & Phillips 1997), whereas ours have $Z = 0.3 Z_{\odot}$. A higher metallicity will increase the fraction of stars in a given galaxy.

Measuring cooled fractions in groups and clusters is difficult, mainly due to the lack of sensitivity in the X-ray instruments to measure hot gas masses out to the virial radius. Current attempts, however (see, for example, the compilation of data by Balogh et al.), measure values between 10 and 20 per cent at 1 keV. These values are marginally consistent with our fiducial result but again a lower ϵ and/or higher metallicity would improve the match.

4 A CLOSER LOOK AT THE MODEL

Given the ability of our fiducial model to adequately reproduce many of the key X-ray observations of groups, we now investigate how these results depend on the strength of the feedback. To facilitate this task we have run a set of smaller simulations (Table 1) with $N = 2 \times 64^3$ particles within a comoving box of length $25 h^{-1}$ Mpc, thus keeping the resolution constant.

After generating group catalogues for each simulation, we also compare the properties of the haloes in two models on an object-by-object basis. To do this we first found the closest pair, then rejected those that had masses differing by more than 15 per cent or separations greater than 20 per cent of the average virial radius. These criteria find a good match for the majority of the haloes in the two catalogues.

4.1 Cooling versus heating

The first comparison we make is between the fiducial model (which has strong feedback) and a run with no feedback at all (the radiative model). This allows us to quantify the relative effects of heating and cooling on the X-ray properties of the groups. In particular, we are interested in knowing whether the model behaves like that proposed by Voit & Bryan (2001), i.e. cooling generates the entropy excess by removing hot gas, which then either forms stars or is reheated and transported to larger radii. If the fiducial model does behave in this

Table 1. Simulations used to study the effects of feedback. From left to right, each column gives the model studied, feedback efficiency, reheating temperature, global fraction of baryons in stars at $z = 0$ and whether the model provides a reasonable match to the L_x-T_x relation.

Model	ϵ	$kT_{\text{SN}}/\text{keV}$	f_{star}	$L_x-T_x?$
Radiative	N/A	N/A	0.15	Yes
Feedback	1	0.1	0.10	No
Feedback	0.1	2	0.12	Yes
Feedback	1	2	0.05	Yes
Feedback	2	2	0.03	Yes

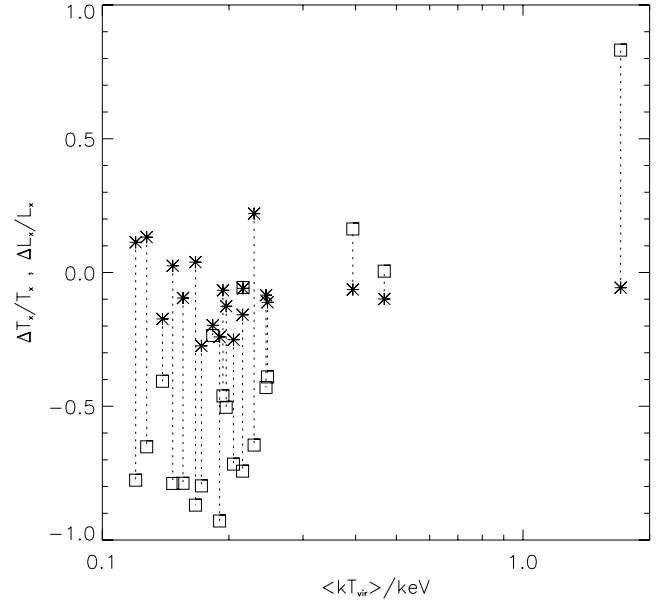


Figure 9. Fractional difference in X-ray temperature (stars) and luminosity (squares) between matched haloes in the simulations with and without feedback, as a function of virial temperature. Dotted lines are a guide to the eye.

way, we expect the feedback only to reduce the fraction of galactic material, leaving the hot gas fraction (and hence X-ray properties) intact.

Indeed, the L_x-T_x relation for the radiative simulation is similar to the fiducial feedback relation, but the former is flatter. This effect is quantified in Fig. 9, where we plot the fractional difference in X-ray temperature (stars) and luminosity (squares) between matched haloes in the two runs against their average virial temperature. These differences are defined as

$$\Delta T_x / T_x = 1 - T_x(\text{feedback}) / T_x(\text{radiative}) \quad (9)$$

and

$$\Delta L_x / L_x = 1 - L_x(\text{feedback}) / L_x(\text{radiative}). \quad (10)$$

There is no strong variation in the difference between X-ray temperatures with system size, although there is a correlation in the X-ray luminosity difference. For $kT_{\text{vir}} \sim 0.1$ keV the objects in the radiative simulation are nearly twice as luminous as those in the feedback run, but the opposite is the case for systems that are a factor of 10 hotter. (Note that because of the small size of the simulations, there is only one halo with $kT_{\text{vir}} > 1$ keV.)

On closer inspection, the trend in luminosity difference is down to two effects caused by feedback. The first, which particularly affects low-mass systems, is a reduction in the mass of hot gas in groups in the feedback simulation, which was inside the virial radius in the radiative simulation. This can be attributed to the increase in pressure from the outflowing reheated material. Secondly, part of the reheated gas, which formed stars in the radiative simulation, is still within the virial radius in the feedback simulation. As the gravitational energy of the halo becomes comparable to that given to reheated gas (i.e. $T_{\text{vir}} \rightarrow T_{\text{SN}}$), the second effect dominates over the first, eventually causing the feedback to increase the X-ray luminosity of a group.

To summarize, we find that our model does behave like that proposed by Voit & Bryan (2001) if $T_{\text{SN}} \sim T_{\text{vir}}$. If $T_{\text{SN}} \gg T_{\text{vir}}$ then feedback also removes hot halo gas (in addition to expelling

reheated material) and so reduces the X-ray luminosity of the group further. Conversely, if $T_{\text{SN}} \ll T_{\text{vir}}$, some reheated gas does not gain enough entropy to escape and so boosts the X-ray luminosity of the group.

4.2 Varying the model parameters

We now investigate the effects of varying the feedback model parameters, ϵ and T_{SN} on the X-ray properties of groups. Given the simplicity of the model, and the results from the previous comparison with a radiative simulation, we should be able to predict how varying the parameters affects the results.

First of all, we consider the effect of varying the feedback parameters on star formation efficiency. The star formation rate, which determines the amount of energy and metals supplied to the interstellar medium, varies inversely with f_{heat} (equation 3), since more reheated cold gas leaves less material available to form stars. Note $f_{\text{heat}} \propto \epsilon/kT_{\text{SN}}$, so we would expect a smaller energy budget and/or a higher heating temperature to increase the star formation rate.

Fig. 10(a) illustrates star fractions against virial temperature for groups in the radiative model plus feedback models with varying parameter values (given in the legend). As expected, the star fraction increases when decreasing ϵ for fixed kT_{SN} , and the model with $\epsilon = 0.1$ contains approximately the correct amount of cooled material (~ 10 per cent, cf. Fig. 8). The impact of varying ϵ on the total baryon fraction is shown in panel (b). As ϵ is increased, more gas is reheated (at the expense of forming stars) and expelled from each halo, decreasing its baryon fraction.

Contrary to expectations, however, the star fraction increases when kT_{SN} is decreased from 2 to 0.1 keV, with the total baryon fraction of the low-temperature case being similar, on average, to the radiative model. As was found for K2002's thermal feedback model, if $T_{\text{SN}} < T_{\text{vir}}$ for the haloes being studied (as is the case for the $kT_{\text{SN}} = 0.1$ keV model), a substantial fraction of reheated gas is not hot enough⁵ to escape from the gravitational potential, and will instead recoll and boost the star formation rate.

The effect of feedback in the fiducial model was to slightly steepen the L_x-T_x relation that was produced by radiative cooling alone. Fig. 11 illustrates the effect of varying the parameters on the L_x-T_x relation. Although the simulations do not contain enough objects to perform a detailed study of the shape of the L_x-T_x relation, we see from our present results that the overall normalization of the relation is fairly insensitive to ϵ when $T_{\text{SN}} > T_{\text{vir}}$, except that the relation becomes slightly steeper as ϵ is increased from 0 (radiative) to 2. Although the heating temperature is the same in these runs, increasing ϵ increases the amount of outflowing material, thus having a larger impact on the hot gas (as discussed in the previous section). When $T_{\text{SN}} < T_{\text{vir}}$ however, (as is the case with $kT_{\text{SN}} = 0.1$ keV) the luminosities are boosted and temperatures decreased considerably. As was observed from the previous figure, reheated material in the latter run is too cold to completely escape from a group-sized halo: the lack of buoyancy causes this gas to boost the central density, hence boosting its X-ray luminosity and lowering its X-ray temperature.

Although the fiducial run provides the best fit to the observations (at least for low-mass groups), we will show in the next section that the lack of numerical resolution in the smaller objects artificially flattens the relation.

⁵Note, however, that some gas will have been hot enough to escape from progenitor haloes at earlier times.

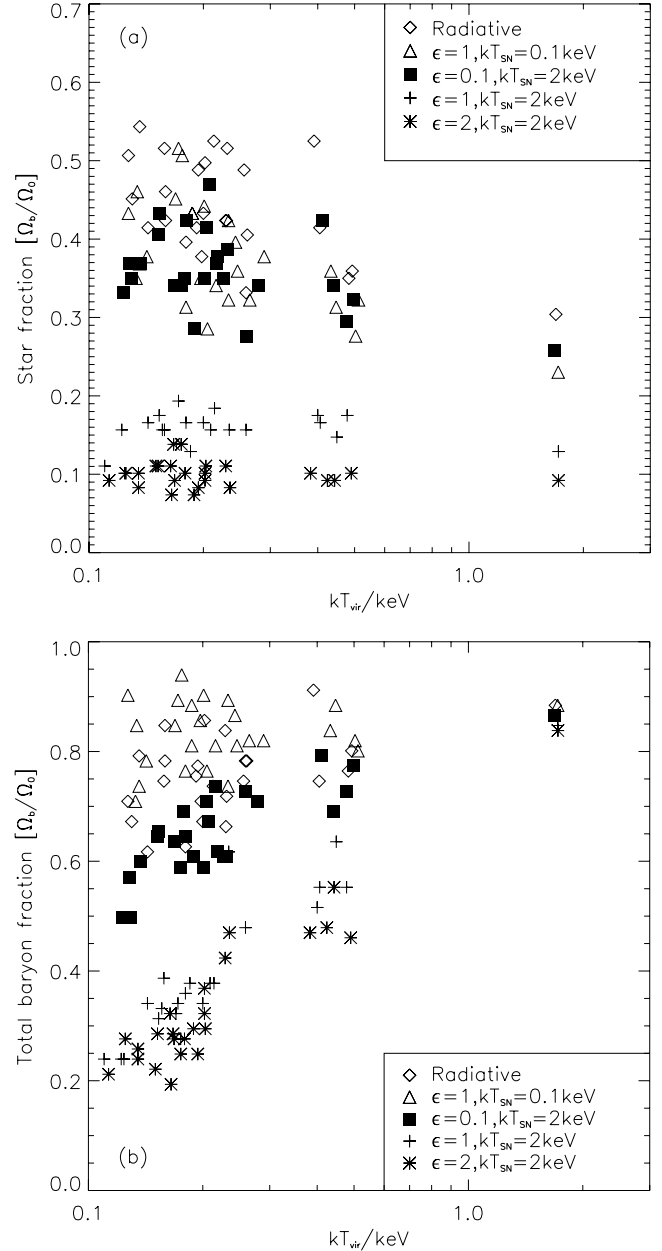


Figure 10. Fraction of baryons in stars (a) and total baryon fraction (b) against the halo virial temperature for the radiative run and the runs with varying feedback parameters.

5 RESOLUTION EFFECTS

The results presented in this paper have all been for fixed resolution. In this section, we present results from a limited study of how varying the resolution affects the X-ray properties of the groups. Table 2 lists properties of the two simulations studied here, a low-resolution simulation (labelled LR) with the same resolution used for the runs studied previously, and a high-resolution simulation (HR) with eight times as many particles. Both runs were performed for a comoving box size of $12.5 h^{-1}$ Mpc and contain the same large-scale power. Although such a box is too small for quantitative predictions, it allows us to compare a small sample of the same objects at different resolution, without requiring a large investment in CPU time. The fiducial feedback parameters were adopted, namely $\epsilon = 2$ and $kT_{\text{SN}} = 2$ keV.

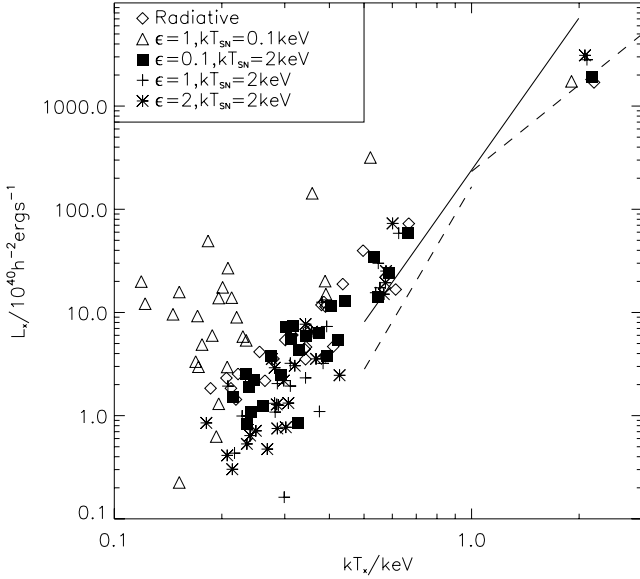


Figure 11. L_x – T_x relations for the radiative simulation and runs with varying feedback parameters.

Table 2. Simulations used to study the effects of varying mass resolution.

Model	N	$m_{\text{dark}}/h^{-1} M_{\odot}$	ϵ_p/h^{-1} kpc	f_{cool}
LR	2×32^3	5.2×10^9	10	0.031
HR	2×64^3	6.5×10^8	5	0.038

The final column in Table 2 lists the cooled baryon fraction for the two runs; a factor of 8 increase in resolution only increases this fraction by ~ 20 per cent. This is because the majority of the mass in galaxies is already resolved at the lowest resolution (i.e. 32 or more particles, the lowest number than can cool efficiently). Furthermore, the feedback acts to stabilize gas cooling since the heating rate is directly proportional to the cooling (star formation) rate. As was stated previously, an overall increase in the cooled fraction must therefore come from choosing a lower value of ϵ and/or a higher metallicity for the cooling gas.

All runs resolve three common objects; the corresponding L_x – T_x ‘relation’ for each simulation is plotted in Fig. 12. Particles from within the cooling radius of each object are excluded from the calculation (which affects only the luminosity of the largest object). Note that the luminosities are more or less unchanged for all three objects when the resolution is varied, due to the stabilizing effect of feedback. For the largest object, which contains between 2800 (LR) and 18 000 (HR) hot gas particles, its X-ray temperature increases only a little, unlike the smaller two objects (between 100 and 1000 particles), where it increases significantly. We therefore expect the slope of the L_x – T_x relation to steepen when the emission-weighted temperatures for all objects have converged.

6 SUMMARY AND CONCLUSIONS

In this paper, we examined the influence of the galaxy population on the X-ray properties of groups at $z = 0$ that form in a cosmological simulation. In particular, we were interested in determining how including feedback of energy from supernovae in the simulations (which decreases the star formation rate) affects the X-ray

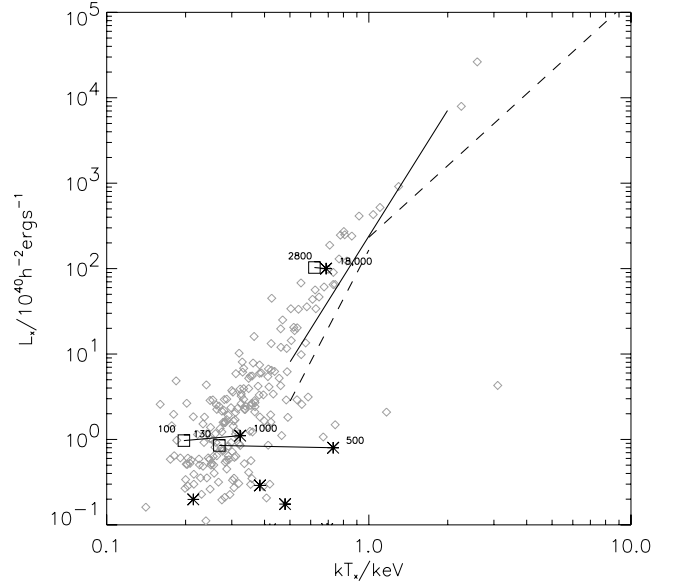


Figure 12. L_x – T_x relation for the groups in run LR (squares) and HR (stars). Matched objects are connected with solid lines. The $N = 2 \times 128^3$ fiducial relation (same resolution as LR) is also plotted (diamonds). Numbers beside each point give the number of hot gas particles within the virial radius of the object. Solid and dashed lines illustrate best-fitting observed relations presented by Helsdon & Ponman (2000) and Xue & Wu (2000), respectively.

properties of the groups. Motivated by the ‘break’ in the X-ray luminosity–temperature relation at the interface between group and cluster scales ($kT_x \sim 1$ – 2 keV), we devised a feedback model based on heating the gas to a fixed temperature, independent of the available energy budget. A given heating temperature, kT_{SN} , and energy budget, ϵ , then determines the star formation rate and the corresponding mass of reheated gas.

For our main results, we studied a model with strong feedback ($\epsilon = 2$, twice the available energy from supernovae) and a heating temperature, $kT_{\text{SN}} = 2$ keV, comparable to the L_x – T_x break. This model generated the required excess entropy in the cores of the groups and so was able to adequately reproduce the X-ray scaling relations over the range of temperatures appropriate to groups ($kT < 2$ keV). However, the fraction of baryons in galaxies was around a factor of 3 lower than observed (assuming a Salpeter IMF).

We then compared our fiducial feedback model to a model with no feedback, and found that the L_x – T_x relations were similar in normalization, but the feedback relation was slightly steeper. Radiative cooling acts to reduce the hot gas fraction (and hence X-ray luminosity) in groups, removing low-entropy material (which forms stars) and causing higher-entropy gas to flow in to replace it. In low-mass groups (where $T_{\text{vir}} < T_{\text{SN}}$), feedback reduces the luminosity further because the outflowing reheated material increases the pressure of the hot gas. However, as $T_{\text{vir}} \rightarrow T_{\text{SN}}$, the effect of feedback on the hot gas diminishes due to the increasing ability of the group to retain a larger fraction of material. As a result, some of the gas that was turned into stars in the radiative run is still within the virial radius in the feedback run, leading to an increase in the luminosities of high-mass groups.

The fraction of reheated material per mass of stars scales as ϵ/kT_{SN} , and so the star formation rate ought to vary inversely with this parameter combination, since more reheated gas leaves less material available to form stars. This is only true if the heating temperature is comparable to or larger than the virial temperature of

the systems being studied. For such a case, decreasing ϵ allows a reasonable match to both the global fraction of baryons in stars and the X-ray properties of the groups. However, when the heating temperature is low compared with the virial temperature of groups (we studied the case when $kT_{\text{SN}} = 0.1$ keV), reheated gas cannot escape from the gravitational potential and instead recools and forms more stars. As a result, this excess of cooling gas decreases the core entropy of the groups and consequently boosts their luminosity.

Finally, increasing the resolution of our simulations appears to have little effect on the X-ray luminosities of groups but the temperatures of the smaller, poorly resolved objects increased. Based on these results, numerical convergence for the range of group masses will act to steepen the L_x - T_x relation.

ACKNOWLEDGMENTS

The work presented in this paper was carried out as part of the programme of the Virgo Supercomputing Consortium (<http://virgo.sussex.ac.uk>). The majority of data were generated using COSMOS, the UK Computational Cosmology Consortium supercomputer, an SGI Origin 3800, at the Department of Applied Mathematics and Theoretical Physics, Cambridge. STK is supported by PPARC; PAT and TT thank PPARC for a Lecturer Fellowship and Advanced Fellowship, respectively.

REFERENCES

- Allen S.W., Schmidt R.W., Fabian A.C., 2002, MNRAS, 328, L37
 Balogh M.L., Pearce F.R., Bower R.G., Kay S.T., 2001, MNRAS, 326, 1228
 Borgani S., Governato F., Wadsley J., Menci N., Tozzi P., Quinn T., Stadel J., Lake G., 2002, MNRAS, 336, 409
 Bower R.G., 1997, MNRAS, 288, 355
 Bower R.G., Benson A.J., Lacey C.G., Baugh C.M., Cole S., Frenk C.S., 2001, MNRAS, 325, 497
 Bryan G.L., 2000, ApJ, 544, L1
 Bryan G.L., Voit G.M., 2001, ApJ, 556, 590
 Cole S. et al., 2001, MNRAS, 326, 255
 Couchman H.M.P., 1991, ApJ, 368, L23
 Couchman H.M.P., Thomas P.A., Pearce F.R., 1995, ApJ, 452, 797
 Davé R., Katz N., Weinberg D.H., 2002, ApJ, 579, 23
 Edmunds M.G., Phillips S., 1997, MNRAS, 292, 733
 Eke V.R., Navarro J.F., Frenk C.S., 1998, ApJ, 503, 569
 Evrard A.E., Henry J.P., 1991, ApJ, 383, 95
 Fukugita M., Hogan C.J., Peebles P.J.E., 1998, ApJ, 503, 518
 Heckman T., 2000, in Hibbard J.E., Rupen M.P., van Gorkom J.H., eds, ASP Conf. Ser., Gas and Galaxy Evolution. Astron. Soc. Pac., San Francisco
 Helsdon S.F., Ponman T.J., 2000, MNRAS, 315, 356
 Hultman J., Pharasyn A., 1999, A&A, 347, 769
 Kaiser N., 1986, MNRAS, 222, 323
 Kaiser N., 1991, ApJ, 383, 104
 Kay S.T., Pearce F.R., Frenk C.S., Jenkins A., 2002, MNRAS, 330, 113 (K2002)
 Kennicutt R.C., 1998, ApJ, 498, 541
 Knight P.A., Ponman T.J., 1997, MNRAS, 289, 955
 Kravtsov A.V., Yepes G., 2000, MNRAS, 318, 227
 Lahav O. et al., 2002, MNRAS, 333, 961
 Lia C., Portinari L., Carraro G., 2002, MNRAS, 330, 821
 Lloyd-Davies E.J., Ponman T.J., Cannon D.B., 2000, MNRAS, 315, 689
 McKee C.F., Ostriker J.P., 1977, ApJ, 218, 148
 Monaghan J.J., 1992, ARA&A, 30, 543
 Muanwong O., Thomas P.A., Kay S.T., Pearce F.R., Couchman H.M.P., 2001, ApJ, 552, L27
 Muanwong O., Thomas P.A., Kay S.T., Pearce F.R., 2002, MNRAS, 336, 527 (M2002)
 Pearce F.R., Thomas P.A., Couchman H.M.P., Edge A.C., 2000, MNRAS, 317, 1029
 Pen U.-L., 1999, ApJ, 510, L1
 Pettini M., Shapley A.E., Steidel C.C., Cuby J., Dickinson M., Moorwood A.F.M., Adelberger K.L., Giavalisco M., 2001, ApJ, 554, 981
 Ponman T.J., Cannon D.B., Navarro J.F., 1999, Nat, 397, 135
 Portinari L., Chiosi C., Bressan A., 1998, A&A, 334, 505
 Raymond J.C., Smith B.W., 1977, ApJS, 35, 419
 Refregier A., Rhodes J., Groth E.J., 2002, ApJ, 572, L131
 Schaye J., Rauch M., Sargent W.L.W., Kim T.-S., 2000, ApJ, 541, L1
 Seljak U., 2002, MNRAS, 337, 769
 Springel V., Hernquist L., 2002, MNRAS, 333, 649
 Springel V., Hernquist L., 2003, MNRAS, 339, 289
 Springel V., White S.D.M., Tormen G., Kauffmann G., 2001, MNRAS, 328, 726
 Steinmetz M., White S.D.M., 1997, MNRAS, 288, 545
 Sutherland R.S., Dopita M.A., 1993, ApJS, 88, 253
 Theuns T., Leonard A., Efstathiou G., Pearce F.R., Thomas P.A., 1998, MNRAS, 301, 478
 Theuns T., Viel M., Kay S., Schaye J., Carswell R.F., Tzanavaris P., 2002, ApJ, 578, L5
 Thomas P.A., Couchman H.M.P., 1992, MNRAS, 257, 11
 Thomas P.A., Muanwong O., Kay S.T., Liddle A.R., 2002, MNRAS, 330, L48
 Thornton K., Gaudlitz M., Janka H.-Th., Steinmetz M., 1998, ApJ, 500, 95
 Voit G.M., Bryan G.L., 2001, Nat, 414, 425
 Voit G.M., Bryan G.L., Balogh M.L., Bower R.G., 2002, ApJ, 576, 601
 White S.D.M., Rees M.J., 1978, MNRAS, 183, 341
 Wu X.-P., Xue Y.-J., 2002a, ApJ, 569, 112
 Wu X.-P., Xue Y.-J., 2002b, ApJ, 572, L19
 Wu K.K.S., Fabian A.C., Nulsen P.E.J., 2000, MNRAS, 318, 889
 Wu K.K.S., Fabian A.C., Nulsen P.E.J., 2001, MNRAS, 324, 95
 Xu H., Jin G., Wu X.-P., 2001, ApJ, 553, 78
 Xue Y.-J., Wu X.-P., 2000, ApJ, 538, 65
 Yepes G., Kates R., Khokhlov A., Klypin A., 1997, MNRAS, 284, 235

This paper has been typeset from a $\text{\TeX}/\text{\LaTeX}$ file prepared by the author.